

Numerical Prediction of Multiphase Flow with Chemisorption

Sumitomo Chemical Co., Ltd.
Ehime Works

Naoki SHIMADA
Tatsuya OZAKI
Process & Production Technology Center
Tetsuya SUZUTA

A new computational fluid dynamics model was developed for applications in compressible bubbly flows with chemisorption by taking into account the component dependence of phase densities. A numerical method for solving the model was then developed. The proposed method was verified through sample calculations, i.e., (1) simulation of a bubbly flow in a uniformly heated column 10 m in height, (2) a bubbly flow with CO₂ absorption in a NaOH solution and (3) chemisorption in a bubble column. As a result, it was confirmed that the proposed method gave good prediction for the effects of pressure, temperature and chemical components on phase densities and for time evaluations of chemical components and gas holdup.

This paper is translated from R&D Report, "SUMITOMO KAGAKU", vol. 2006-I.

Introduction

A chemical apparatus promotes reactions by making good use of flow. For example, a bubble column where the column is full of the liquid phase and bubbles are sparged from the bottom is used in the cyclohexane oxidation process in plants producing caprolactam. The bubbles stir up the liquid phase as they rise, and the reaction progresses because oxygen is supplied to the liquid phase. In evaluating the heat and material balance in such an apparatus, it is important to get a grasp on the state of the flow, but most chemical engineering methods use approximation models for experimental correlative equations and flow. There are limits to the possibilities for the application of these models to the various scales and forms of apparatus as well as the various operating conditions, and this is one factor in making increased precision in the design of chemical apparatus difficult.

Conversely, the space is divided into very small elements (cells) and a conservation equation is solved for each individual cell in a computational model of the flow, as shown in Fig. 1. Therefore, the spatial distribution of the flow can be analyzed in detail, and this model holds possibilities as a design support tool capable of handling the conditions described above.

Sumitomo Chemical Co., Ltd. has jointly developed an $(N+2)$ -field model (NP2 model in the following) with Kobe University, and so far, it has been used in design studies for sparger positioning, container shape and the like in actual bubble columns. On the other hand, one hardly ever sees computational methods that can analyze the flow in a chemical apparatus in a form that completely incorporates the reaction. Therefore, we developed a numerical method that can predict the state of a multi-phase flow accompanying a reaction, interphase mass transfer and heat transport based on the NP2 model.^{1), 2)}

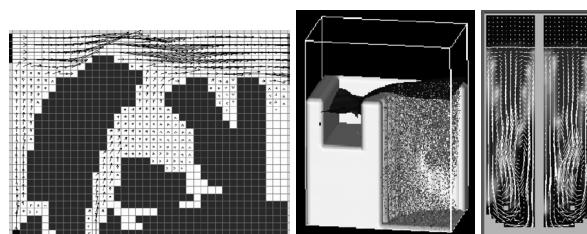


Fig. 1 Examples of computational fluid dynamics

In this paper, we will first give an overview of the method we developed for analyzing flow. Next, we will show the results of an analysis of the gas flow in a column with a thermal load and the process of CO₂ gas

absorption in an aqueous solution of NaOH as examples of applications of this method. In addition, we will introduce an example of analyzing a reaction apparatus using an actual form of bubble column for the process of oxidizing cyclohexane.

Method for Analyzing Flow

1. Computational Model

An NP2 model that can deal with N dispersed phases and two continuous phases can handle a flow that

Table 1 Basic Equations of the proposed model

volume fraction	$\alpha_G + \alpha_L + \sum_{m=1}^N \alpha_{Bm} = 1$
conservative equation of mass	[for bubbles] $\frac{\partial \alpha_{Bm}}{\partial t} + \nabla \cdot (\alpha_{Bm} V_{Bm}) = - \frac{\alpha_{Bm}}{\rho_{Bm}} \frac{D_{Bm} \rho_{Bm}}{Dt} + \frac{1}{\rho_{Bm}} \left(\sum_{m=1}^N \Gamma_{BmBm}^{CB} - \Gamma_{GBm}^{CB} - \Gamma_{LBm}^{AE} \right)$ [for continuous liquid phase] $\frac{\partial \alpha_L}{\partial t} + \nabla \cdot (\alpha_L V_C) = - \frac{\alpha_L}{\rho_L} \frac{D_C \rho_L}{Dt} + \frac{1}{\rho_L} \left(\sum_{m=1}^N \Gamma_{LBm}^{AE} - \Gamma_{GL}^{AE} \right)$ [for continuous gas phase] $\frac{\partial \alpha_G}{\partial t} + \nabla \cdot (\alpha_G V_C) = - \frac{\alpha_G}{\rho_G} \frac{D_C \rho_G}{Dt} + \frac{1}{\rho_G} \left(\sum_{m=1}^N \Gamma_{GBm}^{CB} - \Gamma_{GL}^{AE} \right)$
conservative equation of momentum	[for bubbles] $\frac{\partial V_{Bm}}{\partial t} + V_{Bm} \cdot \nabla V_{Bm} = - \frac{1}{\rho_{Bm}} \nabla P + g - \frac{1}{\rho_{Bm} \alpha_{Bm}} (M_{LBm}^F + M_{LBm}^G)$ [for mixture of continuous phase] $\frac{\partial V_C}{\partial t} + V_C \cdot \nabla V_C = - \frac{1}{\rho_C} \nabla P + F^\mu + F^s + g + \frac{1}{\rho_C \alpha_C} \sum_{m=1}^N (M_{LBm}^F + M_{LBm}^G)$
conservative equation of energy	[for bubbles] $\frac{D_{Bm} T_{Bm}}{Dt} = - \frac{1}{\alpha_{Bm} \rho_{Bm} c_{Bm}^P} \nabla \cdot (\alpha_{Bm} q_{Bm}) + \frac{Q_{Bm}^W + Q_{Bm}^E}{\alpha_{Bm} \rho_{Bm} c_{Bm}^P} - \frac{1}{\alpha_{Bm} \rho_{Bm} c_{Bm}^P} (Q_{LBm}^H + Q_{Bm}^G)$ [for mixture of continuous phase] $\frac{D_C T_C}{Dt} = - \frac{1}{\alpha_C \rho_C c_C^P} \nabla \cdot (\alpha_C q_C) + \frac{Q_C^W + Q_C^E + Q_C^\mu}{\alpha_C \rho_C c_C^P} + \frac{1}{\alpha_C \rho_C c_C^P} \sum_{m=1}^N (Q_{LBm}^H + Q_C^G)$
conservative equation of component	[for bubbles] $\frac{D_{Bm} Y_{Bmi}}{Dt} = \frac{M_{Bmi}}{\alpha_{Bm} \rho_{Bm}} \{ \alpha_{Bm} w_{Bmi} - (1 - Y_{Bmi}) B_{LBmi} \} - \Phi_{Bmi}$ [for continuous liquid phase] $\frac{D_C C_{Li}}{Dt} = \frac{1}{\alpha_L \rho_L} \nabla \cdot (\alpha_L \rho_L D_{Li} \nabla C_{Li}) + w_{Li} + \frac{1}{\alpha_L} \left(\sum_m B_{LBmi} + B_{Ci} \right) + \left[\frac{\partial C_{Li}}{\partial T_C} \frac{D_C T_C}{Dt} + \frac{\partial C_{Li}}{\partial P} \frac{D_C P}{Dt} \right]$ [for continuous gas phase] $\frac{D_C Y_{Gi}}{Dt} = \frac{1}{\alpha_G \rho_G} \nabla \cdot (\alpha_G \rho_G D_{Gi} \nabla Y_{Gi}) + \frac{M_{Gi}}{\alpha_G \rho_G} \{ \alpha_G w_{Gi} - (1 - Y_{Gi}) B_{Ci} \} + \Phi_{Gi}$
equation of state	[for gas phase] $\frac{1}{\rho_k} = \sum_i \frac{Y_{ki}}{\rho_{ki}(P, T_k)}$ [for liquid phase] $\rho_k = \sum_i C_{ki} M_{ki}$
equations for mixture of continuous phase	$\alpha_C = \alpha_G + \alpha_L$ $V_C = V_G = V_L$ $T_C = T_G = T_L$ $\rho_C = \frac{\rho_L \alpha_L + \rho_G \alpha_G}{\alpha_L + \alpha_G}$ $c_C^P = \frac{c_L^P \alpha_L \rho_L + c_G^P \alpha_G \rho_G}{\alpha_L \rho_L + \alpha_G \rho_G}$
subscripts	G = continuous gas phase, L = continuous liquid phase, Bm = bubble group m ($m = 1, 2, \dots, N$), subscripts of Γ = two phase for transfer (e.g. LBm ~ transfer from Bm to L).
variables	α = volume fraction, t = time, V = velocity, ρ = density, Γ^{CB} = mass transfer rate due to coalescence and breakup, Γ^{AE} = mass transfer rate due to absorption and evaporation, P = pressure, g = acceleration of gravity, M_{LBm}^F = force between m^{th} bubble group and liquid, M_{LBm}^G = momentum transfer due to Γ , F^μ = viscous and turbulent diffusion, F^s = surface tension, T = temperature, q = heat flux due to molecular and turbulent diffusion, Q_{LBm}^H = heat transfer between m^{th} bubble group and liquid, Q_{Bm}^G = energy transfer due to Γ_{GBm} , Q^W = work due to pressure, Q^E = other energy source, Q^μ = heat generated by friction, Y = mass fraction, C = molar concentration, w = mole production rate due to reaction, D = diffusion coefficient, B_{LBmi} = component i transfer rate between bubbles and liquid, B_{Ci} = component i transfer rate between gas and liquid, $\Phi_{Bmi} \cdot \Phi_{Gi}$ = component i transfer rate due to Γ_{GBm} , $D_{Bm}/Dt \cdot D_C/Dt$ = material derivative, M = molecular weight

includes interfaces on various scales from particle diameter to an entire apparatus. In addition, if suitable correlative equations are incorporated, it is possible to calculate the flow for a single phase flow, gas-liquid two phase flow, solid-gas two phase flow, gas-liquid-solid three phase flow and gas-liquid-liquid three phase flow, but to make matters simple in this paper, the flow will be limited to a gas-liquid two phase flow.

Processes for handling chemical substances involve various reactions, interphase mass transfer, temperature changes and pressure changes. Therefore, when we predict numerical values in a chemical apparatus, we must consider the temperature, pressure and chemical component dependence of density, and must use conservative equations for mass, momentum, energy and chemical concentration and equations of state for the flow of each phase as basic equations. The model we propose classifies the phases into the continuous gas phase (subscript G), continuous liquid phase (L), and bubble group N (Bm) shown in Fig. 2, and the basic equations are given in Table 1.

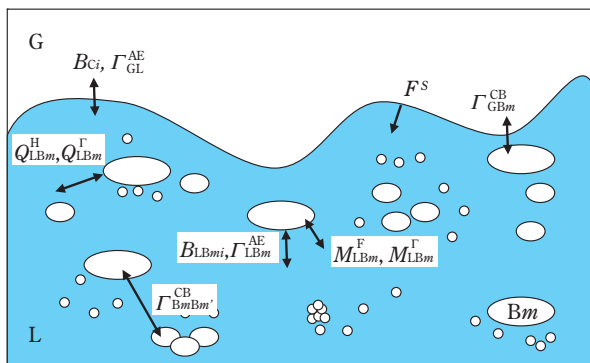


Fig. 2 Phase classification in NP2 model²⁾

2. Numerical Solution Procedure

When numerical integration is carried out on the basic equations in the previous section based on a numerical solution procedure for a compressed flow, the time division width Δt is restricted by Courant-Friedrichs-Levy (CFL) conditions.³⁾

$$\frac{(a+V)\Delta t}{\Delta x} \leq \frac{1}{3} \quad (\text{Eq. 1})$$

Here, a is the speed of sound, V the maximum velocity in the flow field and Δx the grid scale. These are the restrictions for an explicit scheme for Eq. 1, but even when a semi-implicit scheme or a completely implicit scheme is used, it has been pointed out that a conver-

gent iterative solution cannot be obtained if CFL conditions are not satisfied when iterative computations are carried out with the simultaneous equations making up the implicit scheme.³⁾ On the other hand, when numerical integration is carried out on an incompressible fluid using standard computational methods such as SMAC,⁴⁾ SIMPLE⁵⁾ and the like, Δt is restricted by the following Courant conditions.

$$\frac{V\Delta t}{\Delta x} \leq \frac{1}{3} \quad (\text{Eq. 2})$$

In two phase flows such as a gas bubble flow in a gas bubble column, a is around 100 times V , so Δt in the calculations of compressible fluid is around 1/100 of Δt the uncompressed flow. This requires a large amount of computation time for calculations for a compressible three-dimensional multi-phase flow on a large scale, and it is extremely difficult to actually obtain a solution. For the reasons given above, most three-dimensional thermal flow calculations used at present are carried out based on basic equations for incompressible fluid.

To overcome this problem, we developed an efficient numerical solution procedure for reactive flows. First, we constructed a method for solving the basic equations for a compressible fluid based on the solutions proposed by Tomiyama et al.,⁶⁾ so that the temperature and pressure dependence of density could be handled.

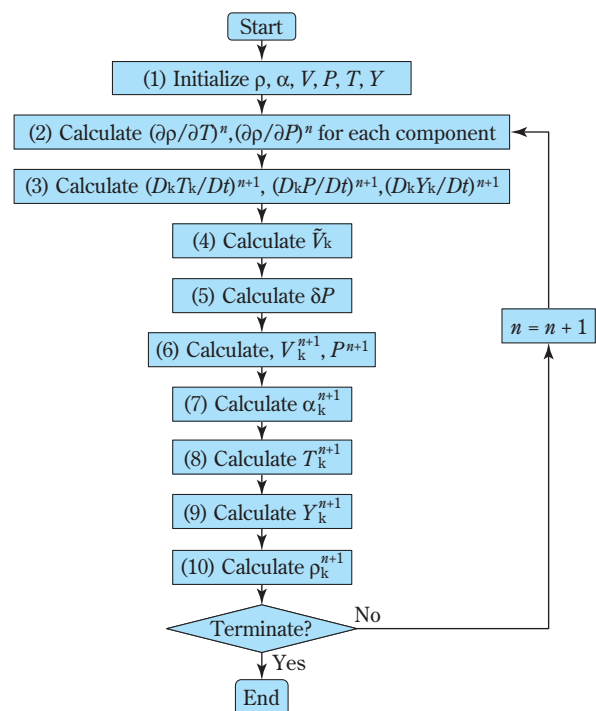


Fig. 3 Solution Procedure

With this method of solution, fluid analysis that includes equations of state became easy. Next, this model was extended to multi-component systems and was made to handle the temperature, pressure and chemical components dependence of density. In addition, by using a semi-implicit scheme for interphase heat and mass transfer and chemical reaction calculations, we avoided instability and errors in the calculations. The calculation procedure is outlined in Fig. 3.

Because of space limitations here, see the references^{1), 2)} for details of the solution method. Following calculations of velocity and pressure field [Fig. 3 steps (2) – (6)], this numerical method can be constructed in a framework for incompressible fluid using volume fraction, temperature, chemical type and density calculation steps [Fig. 3 steps (7) – (10)], and program modification is also easy.

Examples of Application

1. Bubbly Flow in a Column with Thermal Load

First, as an example of applying the proposed numerical solution method, we examined the changes in the volumetric flux for each phase due to the lowering of pressure and increase in temperature when a thermal load from the walls of the column was applied to a bubble flow in a column with a cross-sectional area of 0.01m^2 and a height of 10m. Both the gas and liquid phases flow in from the bottom and flow out from the top. The mass flow rate of the gas is $9.4672 \times 10^{-3}\text{kg/s}$, and the mass flow rate of the liquid is 0.479kg/s . The bubble diameter at the inflow is 3mm, the temperature at the inflow 20°C and the thermal dose 15kW . The calculation results are shown in Fig. 4. The lines in the figure are, from the top, axial (z) distributions of average cross-sectional liquid temperature, average cross-sectional gas volumetric flux and average cross-sectional liquid volumetric flux. With this target, applying pressure and changing the temperature affects the changes in the volumetric flux for each phase. Since we let the thermal flux from the walls be uniform, the average cross-sectional temperature is found using the following equation.

$$T_c = T_d = T_{in} + \frac{\Delta Q_E}{c_{pL}W_{cL} + c_{pd}W_d} z \quad (\text{Eq. 3})$$

Here, T_{in} is the inlet temperature, W_{cL} the liquid mass flow rate and ΔQ_E the thermal dose per unit length in the z direction. The values from Eq. (3) (cir-

cles in the graphs in Fig. 4) and the results of the calculations agree very well, and we can see that this method achieves conservation of energy. In addition, an evaluation can be made by using the average cross-sectional gas volumetric flux J_d in the following equation.

$$J_d = \frac{W_d}{\rho_d} = \frac{W_d RT_d}{P_{in} - \bar{\rho}_{cL} (1 - \bar{\alpha}_d) gz} \quad (\text{Eq. 4})$$

Here, $\bar{\rho}_{cL}$ is the average liquid density in the area from the inlet to position z . Since the temperature change for this target is 30°C , the change in the liquid density is small at approximately 1%. Therefore, the effect of the change in liquid density on the pressure distribution is small. Thus, we evaluated the cross-sectional average gas volumetric flux letting $\bar{\rho}_{cL}$ be constant in Eq. 4 and using the liquid density at the inlet as a typical value. On the other hand, an evaluation can be made by using the average cross-sectional liquid volumetric flux J_c in the following equation.

$$J_c = \frac{W_{cL}}{\rho_{cL}} \quad (\text{Eq. 5})$$

Here, the temperature necessary for the liquid phase density calculation is found using Eq. (3). The results of calculations for J_d and J_c in Fig. 4 agree well with the approximation using Eqs. (3) – (5), so it is possible to confirm that the method of solution proposed can accurately evaluate the temperature and pressure dependence of fluid density.

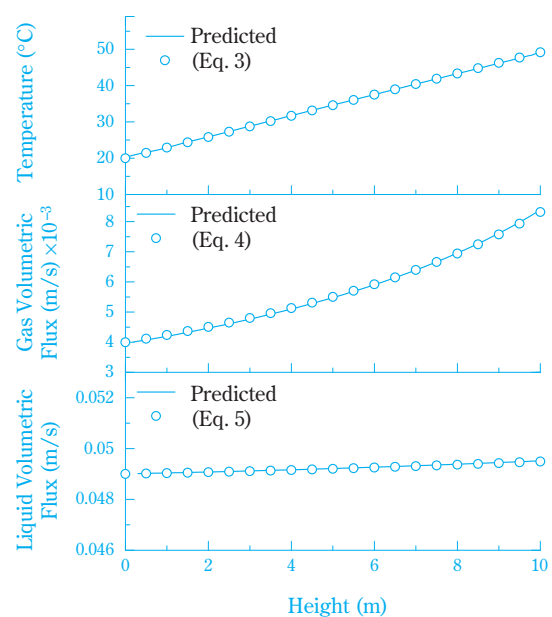


Fig. 4 Axial profiles of temperature, gas volumetric flux and liquid volumetric flux¹⁾

2. CO₂ Gas Absorption Process in Aqueous Solution of NaOH

Fleischer *et al.* (1996)⁶⁾ have carried out experiments on CO₂ gas absorption in an aqueous solution of NaOH using a bubble column. They reported that when the pH is high (pH > 13) after starting the bubble flow, the bubbles are completely dissolved in the liquid, but as the pH drops because of the reaction, the bubbles move to a flow where they reach the top of the apparatus. Therefore, we verified this procedure under the conditions of an apparatus with a cross-section and empty column rate identical to their experiment.

We considered nitrogen (N₂) and carbon dioxide (CO₂) for the bubbles and continuous gas side composition and water (H₂O), carbon dioxide (CO₂), sodium ions (Na⁺), hydroxide ions (OH⁻), hydrogen carbonate ions (HCO₃⁻) and carbonate ions (CO₃²⁻) for the liquid side composition. The reaction that occurs between NaOH and CO₂ in the liquid is included in the reaction equation in Table 2.⁷⁾ The density of the discrete phases and continuous phases is evaluated using an equation of state for an ideal gas. In addition, since the mole concentration of H₂O on the liquid side is sufficiently large in comparison with the other chemical species, we only considered the temperature dependence of the H₂O mole concentration. Furthermore, a viscosity equation for H₂O was used to evaluate the liquid viscosity. The DIPPR database of physical properties was used to evaluate the physical properties of pure substances other than these.

Table 2 Parameter values for chemical reaction

	Reaction	Kinetic constant (m ³ /s)	Equilibrium constant (m ³ /mol)
I	CO ₂ + OH ⁻ ⇌ HCO ₃ ⁻	5.0	6.1 × 10 ⁴
II	HCO ₃ ⁻ + OH ⁻ ⇌ CO ₃ ²⁻ + H ₂ O	1 × 10 ⁴	5.88

Fig. 5 shows a schematic of the apparatus. The apparatus has a square cross-section of 0.08m × 0.08m, and the surface of the liquid is positioned at a height of 0.4m from the bottom. Gas bubbles of 99.9wt% CO₂ and 0.01wt% N₂ are injected from a sparger positioned 0.02m from the bottom. The superficial velocity was set at 0.008m/s, the initial bubble diameter 4mm and initial pH 13.3 (NaOH mole concentration of 200mol/m³). The measured value of 0.0346 atm m³ mol⁻¹ was used for the Henry constant.^{7), 8)} In the calculations 8 × 8 × 45 = 2880 cubic cells of Δx = Δy = Δz =

0.01m were used. When calculations were done from t = 0 to 350 sec, the calculation time required approximately 80 hours on personal computer (CPU: Pentium IV 2.8 GHz, Memory: 1 GHz).

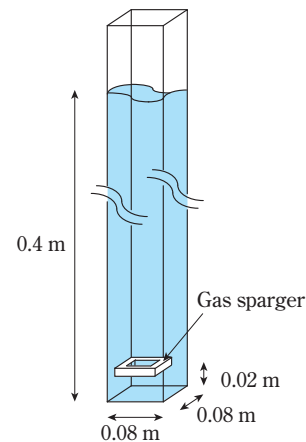


Fig. 5 Geometry of a bubble column²⁾

Fig. 6 (a) shows the void fraction distribution and the pH distribution changes over time. Up to 90 sec after inflow is started the CO₂ is completely absorbed in an area within approximately 0.2m from the inlet, and the void fraction in the upper part approaches 0. With the passage of time, the pH drops, and the void fraction increases, widening the range. This is because the absorption rate drops dependent on the pH. The pH drops faster as the void fraction in the area becomes greater, but since the gas flow mixing effect is large, the lower pH area spreads into areas where there are no bubbles. Fig. 6 (b) shows the changes in the CO₂ mole concentration in the liquid over time. Since the dissolving process is rate determining, the CO₂ that moves into the liquid is rapidly consumed by the reaction. Therefore, the change in CO₂ mole concentration distribution on the liquid side behaves in a manner similar to the void fraction. When the system is accompanied by reaction heat, density changes caused by changes in temperature occur, and a natural convective effect is added. To take this effect into consideration, the enthalpy arising in the reaction is given as an energy source for performing the calculation. The changes in the liquid temperature distribution over time are shown in Fig. 6 (c). Since the mixing effect due to the bubble flow and natural convection is large, the difference in temperature within the system in the process of increasing the temperature is 1.5 °C or less.

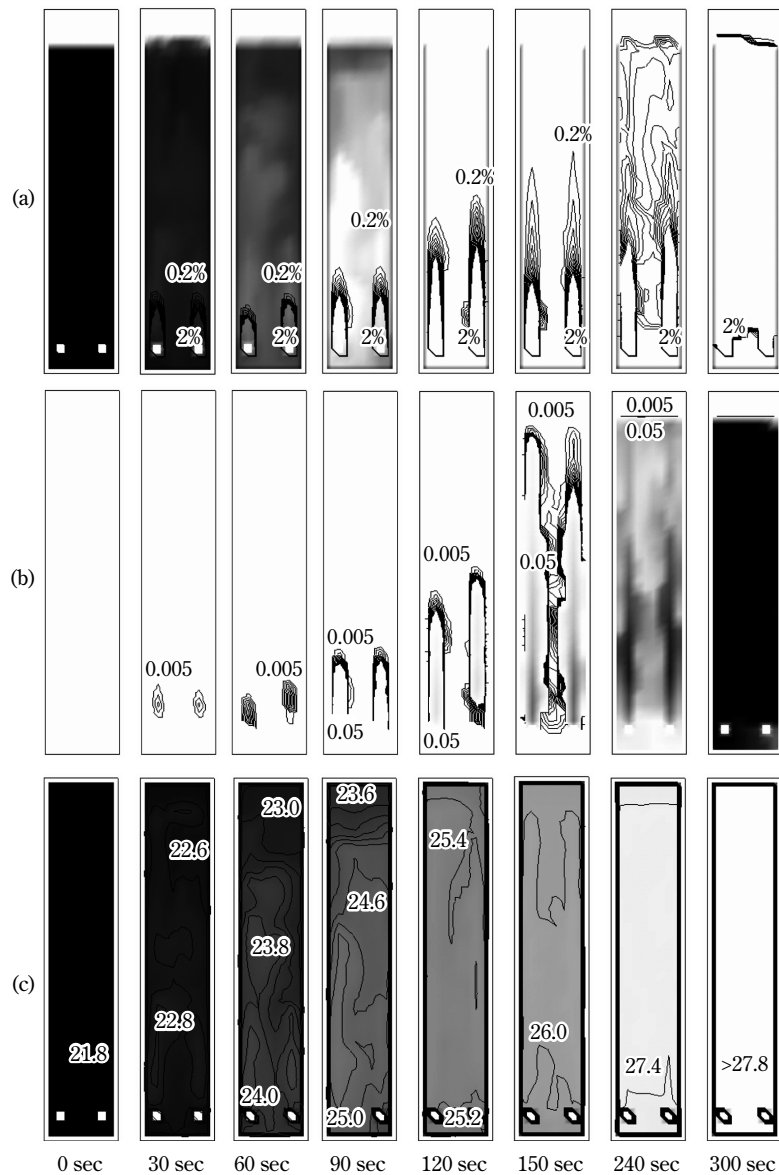


Fig. 6 Transient pattern of CO₂ chemisorption, (a) pH and void fraction (color : pH 12.5 (white) – 13 (black), contour line: void fraction, 0.2% × 10 lines), (b) mole concentration of CO₂ in liquid phase (color : 0 (white) – 5 (black) mol/m³), (c) temperature of continuous phase (color : 21.8 (black) – 27.8 (white) °C)²⁾

Fig. 7 shows the changes in average pH in the apparatus over time. After OH⁻ is consumed by reactions I and II in Table 2 in the initial stages, the reverse of reaction II temporarily becomes larger, and as a result of the subsequent resumption of OH⁻ consumption, the pH drops in two steps.⁶⁾ The circles in Fig. 7 show the results of the experiments by Fleischer *et al.* (1996). Since the liquid volume in the calculations here is smaller than that in the experiments, we multiplied the time for the experimental results by the volume ratio for the comparison. As a result of the comparison, we found that the drop in the pH in the calculations was more rapid than in the experiments. This is mainly because the combined fraction for the bubbles increases with the increase in the void fraction in the

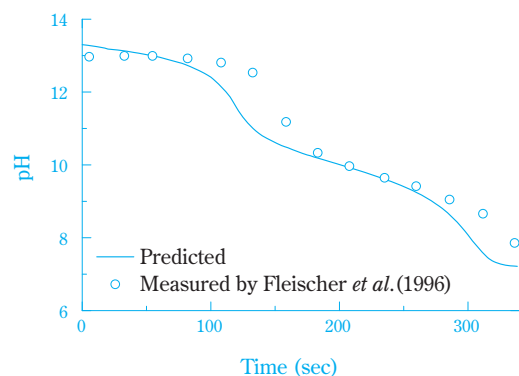


Fig. 7 Transient pattern of average pH²⁾

experiment while only the effect of the decrease in the bubble diameter due to gas absorption was considered in the calculations, so the absorption is lower than cal-

culated. Fleischer *et al.* (1996) also have reported from the results of observations that as the pH drops, there is an increase in the proportion of large bubbles present.

3. Reaction Process Using and Actual Form of Bubble Column

Fig. 8 arranges the input and output variables when this procedure is used for calculations for a reaction process. Input information such as the shape of the apparatus, amount of flow, physical property values (equations of state and the like) are necessary for the calculations. In addition, correlative equations must be selected according to the state of the flow. After the calculations, a three-dimensional distribution of the composition in the apparatus, flow rate, pressure and energy is output. In particular, from the values at the outflow, we can obtain a performance evaluation for the apparatus in the reaction rate, selection rate, basic units, changes in pressure, changes in temperature and the like.

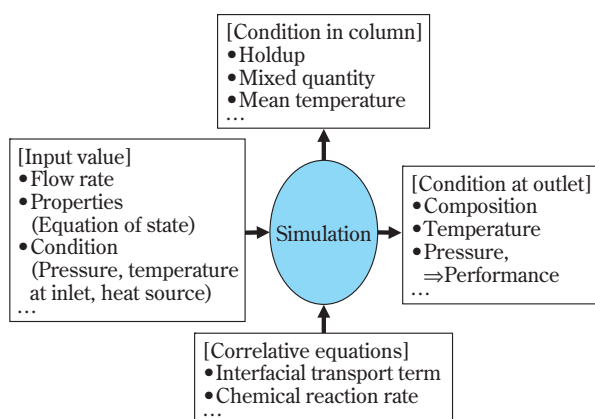


Fig. 8 Simulation strategies for practical plants

We used a cyclohexane oxidation process as an example of a reaction process using an actual form of bubble column. This process is one example for which numerical calculations for the flow were given by the sparger position and the design of the container shape up to this point. There is a complex, multi-stage free radical chain reaction, and it is made up of various chain restrictions, chain propagations and chain termination stages. As a guideline for a reaction model in industrial apparatus for this reaction, Pohorecki *et al.* (2001)⁹ have indicated that “In actual calculations, a large number of reaction rate constants are required for systems that are too complex, and it becomes

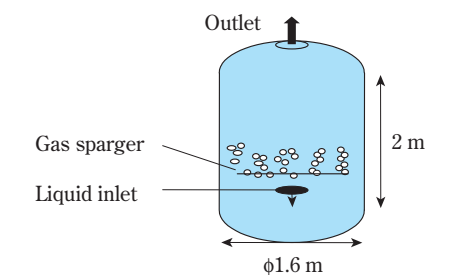
impossible for sufficient precision to be established at the same time. Requiring rate constants on the order of ten is reasonable.” Unfortunately, the reaction models have not been sufficiently publicized at present. Here, we incorporated the ten equations¹⁰ given in Table 3 as reaction equations for which reaction rate constants are clearly defined. We considered cyclohexane (CHX), cyclohexylhydroperoxide (HPO), cyclohexanol (AL), cyclohexanone (AN), two radicals (RO₂* and R*), byproducts (D) and oxygen (O₂) for the components on the liquid side, and nitrogen and oxygen on the gas side. We made only oxygen move from the gas side to the liquid side made the reaction occur in the liquid. Moreover, the application of quasi-steady state approximations and consideration of catalytic dependence⁹ for free radicals, which cannot be measured directly, are a topic for the future.

Table 3 Parameter values for cyclohexane oxidation

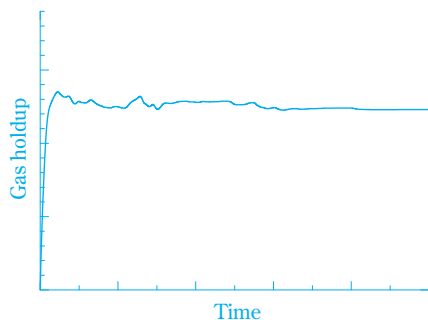
No.	Reaction	Reaction rate
1	CHX + O ₂ → R* + RO ₂ *	0.0266
2	R* + O ₂ → RO ₂ *	1.0 × 10 ⁹
3	CHX + RO ₂ * → HPO + R*	9.3
4	2RO ₂ * → AN + AL + O ₂	1.55 × 10 ⁶
5	2RO ₂ * → D	0.2 × 10 ⁶
6	HPO → AL + 0.5O ₂	0.0048
7	HPO → AN + D	0.0013
8	AL + 0.5O ₂ → AN + H ₂ O	0.5
9	AN + 1.5O ₂ → D	0.37
10	HPO → RO ₂ * + D	1.5 × 10 ⁻⁴

The container shown in Fig. 9 (a) with an inside diameter of 1.6m and straight cavity length of 2m (volume of approximately 6m³) was used for the reaction vessel. One liquid supply nozzle and one gas sparger are provided inside, and both the gas and liquid flow out of the top of the column. A liquid of 100% cyclohexane and gas bubbles of 80% nitrogen and 20% oxygen were set for the compositions supplied.

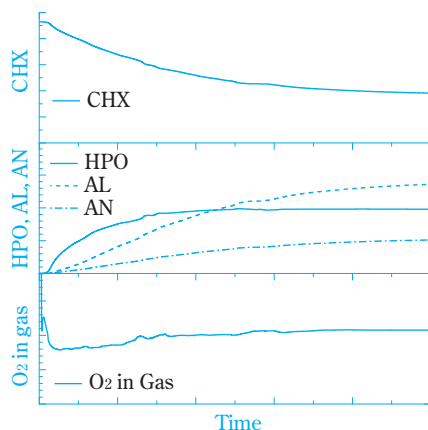
Fig. 9 (b) and (c) show an example of the results of calculations of the changes in each chemical species in the gas hold-up and outflow over time. We found that because the column is small, the changes over time are small and there is stability inside the column. Furthermore, by varying the flow rate for the gases and liquid supplied and examining the gas absorption rate and liquid composition at the outflow, we can evaluate the performance of the apparatus. Fig. 9 (d) shows the



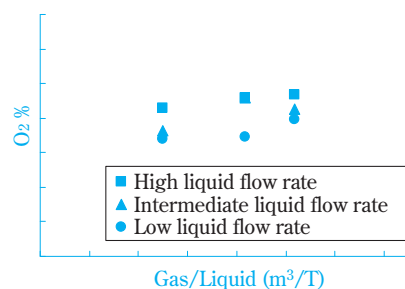
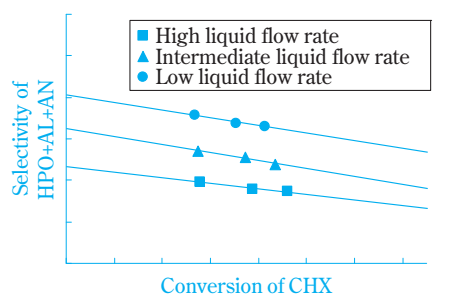
(a) Schematic of apparatus



(b) Time evolution of gas holdup



(c) Time evolution of components at outlet

(d) Mass fraction of O₂ in exhaust gas

(e) Relation between conversion and selectivity

average mass fraction for oxygen in the bubbles at the outflow (called exhaust gas oxygen concentration in the following). In this example, there is an increase in the oxygen concentration in the exhaust gas with an increase in the flow rate. On the other hand, there is an increase in the gas absorption with a decrease in the liquid flow rate, and the oxygen concentration in the exhaust gas drops. Fig. 9 (e) shows the relationship between the predicted cyclohexane conversion rate and selectivity of products (HPO + AL + AN). The conversion rate and selectivity rate do not have a one-to-one relationship, but rather we must be careful of the point that it changes according to the amounts of gas and liquid supplied.

It is known that in reactions where the target is an intermediate product in a successive reaction like the cyclohexane oxidation reaction, selectivity is affected by the state of the flow.¹¹⁾ The only time that the conversion rate and selectivity rate can be arranged in a one-to-one relationship is when the state of flow does not change at all (for example, when complete mixing is always assumed), and it is difficult to make this assumption for most chemical apparatus. Furthermore, the flow accompanying reactions is a dynamic phenomenon, and there are limits to approaches based only on equilibrium theory.¹¹⁾

Conversely, this technique, directly evaluates the dynamic effects of a wide variety of apparatus scales, shapes and operating conditions on heat and mass balances.

Conclusion

This paper has introduced a method for analysis that can predict multi-phase flows that accompany reactions, interphase mass transfer and heat transport based on the an $(N+2)$ -field model. This numerical computation method can be constructed within the framework of existing solutions for incompressible fluid, and the program can easily be modified. Because of these characteristics, we have become more familiar with calculations of flow states in reaction apparatus using a personal computer. We verified that the method we have proposed can accurately evaluate the temperature, pressure and chemical species dependence of fluid density and can directly evaluate the dynamic effects of apparatus scale and shape and operating conditions on the heat and mass balance by making applications to multiple targets.

Fig. 9 Simulation of cyclohexane oxidation

References

- 1) N. Shimada, A. Tomiyama, *Kagakukougaku Ronbunshu*, **31** (1), 15 (2005).
- 2) N. Shiamda, A. Tomiyama, M. Maekawa, T. Suzuta, T. Ozaki, *Kagakukougaku Ronbunshu*, **31** (6), 377 (2005).
- 3) A. Tomiyama, Y. Ichikawa, K. Morioka, T. Sakaguchi, *Trans. JSME, Ser. B*, **57** (538), 2054 (1991).
- 4) A. A. Amsden and F. H. Harlow, LA-4370, *Los Alamos National Laboratory Report* (1970).
- 5) S. V. Patankar and D. B. Spalding, *Int. J. Heat Mass. Tran.*, **15**, 1787 (1972).
- 6) C. Fleischer, S. Becker and G. Eigenberger, *Chem. Eng. Sci.*, **51**, 1715 (1996).
- 7) G. Astarita, "Mass transfer with chemical reaction", Elsevier (1967).
- 8) S. Rigopoulos and A. Jones, *Chem. Eng. Sci.*, **58**, 3077 (2003).
- 9) R. Pohorecki, W. Moniuk, P. Bielski, and A. Zdrojkowski, *Chem. Eng. Sci.*, **56**, 1285 (2001).
- 10) R. Pohorecki, J. Baldyga, W. Moniuk, A. Krzysztoforski and Z. Wojcik, *Chem. Eng. Sci.*, **47**, 2559 (1992).
- 11) H. Komiyama, "Sokudoronn", 1st. ed. , Asakura Shoten, (1990), p.1.

PROFILE

*Naoki SHIMADA*

Sumitomo Chemical Co., Ltd.
Ehime Works
Ph. D.

*Tetsuya SUZUTA*

Sumitomo Chemical Co., Ltd.
Process & Production Technology Center
Senior Research Associate

*Tatsuya OZAKI*

Sumitomo Chemical Co., Ltd.
Ehime Works
Senior Staff